Analytical Methods

Accepted Manuscript

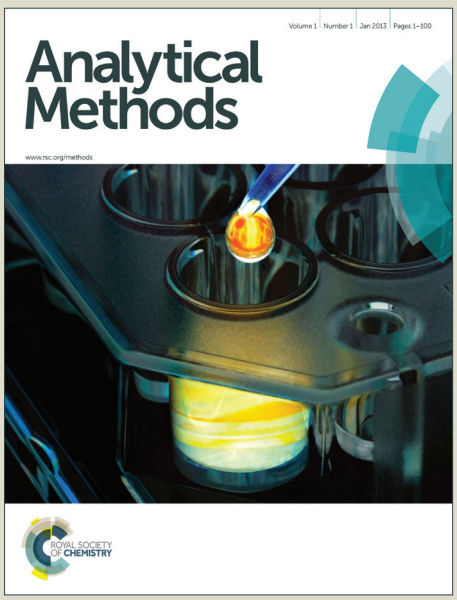

ROYAL SOCIETY OF CHEMISTRY

www.rsc.org/methods

Raman spectroscopy of oral tissues: correlation of spectral and biochemical markers

S.P. Singh[1], C. Murali Krishna[1,*]

[1]Chilakapati Lab, ACTREC, Kharghar, Navi Mumbai - 410210

*Corresponding author:

Dr. C. Murali Krishna

Scientific Officer 'F' and Principal Investigator

Chilakapati Lab

Advanced Centre for Treatment, Research and Education in Cancer (ACTREC)

Tata Memorial Centre (TMC)

Sector '22', Kharghar

Navi Mumbai – 410210, INDIA

Telephone: +91-22-27405039

Email: mchilakapati@actrec.gov.in, pittu1043@gmail.com

Keywords: Raman spectroscopy, Oral cancer, Curve deconvolution, Biochemical correlation.

Abbreviations used: OSCC- Oral squamous cell carcinoma, FTIR-Fourier Transformed Infra Red, RS- Raman Spectroscopy.

Abstract

Both *ex vivo* and *in vivo* Raman spectroscopic studies carried out in oral cancer over the past decade have demonstrated that the spectra of normal tissues are rich in lipids and tumors have predominant protein features. However, in view of variability in Raman scattering cross section of biomolecules, it is pertinent to explore spectral features *viz a viz* biochemical composition in order to verify spectral markers as biochemical markers. Spectra of 20 pairs of normal and tumor oral tissues were acquired using fiberoptic probe coupled Raman-spectrometer. Intensity associated with lipid (1440 cm^{-1}) and protein (1450 and 1660 cm^{-1}) bands were computed and correlated with biochemical estimation for protein, lipid and phospholipid from the same tissues. The intensity of the lipid band was higher in normal tissues while that of the protein band was higher in tumors. Biochemical estimation yielded similar results *i.e.* high protein to lipid or phospholipid ratio in tumors with respect to normal tissues. These differences were found to be statistically significant. Findings of curve-deconvolution and biochemical estimation correlate well and suggest that spectral features are the hallmark of underlying biochemical tissue composition.

1. Introduction

Cancer is the second most common cause of morbidity and mortality in the world today, after cardiovascular disorders. Oral cancer is the eleventh most common cancer in the world, with two-thirds of oral cancers occurring in the developing countries [1,2]. Oral cancers in India accounts for >30% of all cancers as in contrast to USA, where oral cavity cancer represents only ~3% of all malignancies. India tops in the prevalence of oral cancer in the world (accounts for one-third of the global oral cancer burden) and remains the most common cancer among the males and third in females. Tobacco (both smoking and chewing) is regarded as the major cause of oral cancer [3-5].

Early detection and diagnosis is the best means to reduce morbidity due to oral cancer. Screening by visual examination of high risk population lacks accuracy, reproducibility and requires expertise and may be useful only for chronic smokers and alcoholics. A definitive diagnosis is made only after the histopathological examination of a tissue biopsy. However this approach suffers from some of the known limitations like subjectivity, sampling error and patient discomfort, and further it may not be practical for screening [6, 7].

Optical diagnostic methods based on fluorescence, Raman and Fourier transform infrared spectroscopy are being projected as promising new technologies for improving screening and detection of malignancies in several organs [8,9]. These methods are capable of providing biochemical information within a short time frame which can be used for online diagnosis. Among these, Raman spectroscopy with attributes such as negligible water interference, sharp spectral signatures and abundance of Raman active molecules in biological samples holds edge over other methods. Raman spectroscopic differentiation of normal and cancerous conditions of prostate, esophagus, skin, cervix, and other forms of cancer have already been reported in the literature [10-18]. Recent Raman spectroscopic studies, both *ex vivo* and *in vivo*, have demonstrated the efficacy in classifying normal, pre-cancerous and cancerous conditions of oral cavity [19-30]. We have also shown that confounding factor such as cancer field effects and age associated changes in the clinically normal appearing mucosa can be identified [29-30]. *Ex vivo* and *in vivo* Raman spectroscopic studies, carried out over last decade have established that spectra of normal conditions have predominant lipid features while tumors are rich in proteins [21-30]. Absence of a particular biomolecule in the spectra is suggestive of the fact that either they are not present in

sufficient quantity or they lack does not have strong enough Raman scattering cross section (indicates the strength of the signal at unit concentration) to appreciably contribute to the spectrum [31]. Therefore, in view of variability in Raman scattering cross section of biomolecules, it is pertinent to explore Raman spectral features *viz a viz* biochemical composition in order to prove spectral markers are indeed direct biochemical markers. Hence, in the present study, gross spectral features and band intensity parameters derived from curve-deconvolution studies have been correlated with biochemical estimations of same tissues and findings are discussed in the manuscript.

2. Material and Methods

2.1 Clinical samples: The study was approved by the Institutional Ethics Committee, Tata Memorial Centre, Mumbai, India. *Ex vivo* biopsies of buccal mucosa tissues (20 pairs of normal/ histopathologically confirmed tumor tissues) were obtained from the Biorepository, ACTREC. Tumor refers to the tumor tissue obtained during surgical resection of tumor of buccal mucosa. Normal refers to the normal buccal mucosa tissue adjacent to the tumor obtained during surgical removal of margins. Two frozen sections, each of 5-μm thickness cut longitudinally by orienting epithelium and connective tissue in order, were used for histopathological certification. The remaining tissue was placed on a CaF_2 window and used for recording Raman spectra.

2.2 Raman spectroscopy: Spectra from the *ex vivo* biopsies were acquired with a fiberoptic probe (RPS 785/12-5, InPhotonics Inc., Downey St., USA) coupled HE-785 commercial Raman spectrometer (Jobin-Yvon-Horiba, France). An elaborate description of the instrument is given elsewhere [25-30]. Briefly, the instrument consists of a diode laser (PI-ECL-785-300-FC, Process Instruments) of 785 nm wavelength as the excitation source, a high efficiency (HE-785, HORIBA Jobin Yvon, France) spectrograph with fixed 950 gr/mm grating coupled with CCD (CCD-1024X256-BIDD-SYN, Synapse) as the detection components. The probe consists of 105-µm excitation fiber and 200-µm collection fiber (NA-0.40). As per specifications of manufacturer of the Inphotonics probe, theoretical spot size is 105 µm. The spectral resolution as per manufacturer's (HORIBA Jobin Yvon, France) specification is ~4 cm^{-1}. Passively thawed samples were placed on a CaF_2 window and spectra were acquired at different points with spacing of ~1-2 mm using XYZ precision stage. On an average, 8 spectra were acquired from each tissue. Spectral acquisition parameters were: λ_{ex} -785nm, laser power-52 mW, integration

time-10 seconds and accumulations-5. These parameters were kept constant during all measurements and tissues were kept moist with saline to prevent desiccation.

2.3 Data analysis

2.3.1 Spectral pre-processing: Raman spectra were corrected for CCD response with a NIST certified SRM 2241 material followed by subtraction of the background signals from optical elements. Spectra were baseline corrected by fitting 5th order polynomial function followed by smoothening (Savitzky-Golay method and window size 3) and vector normalization. Mean or average spectra were computed by averaging variations on the Y- axis, keeping the X- axis constant.

2.3.2 Curve deconvolution: The pre-processed, baseline corrected spectra were resolved into individual component bands using curve deconvolution technique, based on the original algorithm of Levenberg-Marquardt [32-35]. In this method, the sum of the squared differences between observed and computed spectra are minimized to get the best fit. The spectral region 1200 to 1800 cm^{-1} was used for the deconvolution analysis. Normal and tumor oral tissue spectra were resolved into 8 and 9 bands, respectively. Each band is characterized by four parameters: shape factor, peak position, peak intensity and full width at half maximum (FWHM). The shape factor decides the band shape. In our deconvolution analysis, the Gaussian band led to the best fit. In order to understand the relative distribution of biomolecules, we have also generated scatter intensity plots by computing the area under each of the fitted bands (integrated intensity).

2.3.3 Statistical analysis: The data were expressed as mean $\pm$ standard deviation (SD), and statistical comparisons were performed by unpaired student's t-test. p value <0.05 was considered statistically significant, $p < 0.01$ as highly significant and $p < 0.001$ as very highly significant.

2.4 Biochemical estimations

Following spectral acquisition, each tissue was divided in two parts. One part was homogenized in appropriate buffer and processed for protein estimation. Other part was homogenized in alcohol/acetone solution and utilized for total lipid and phospholipid estimation. Estimation of total protein, total lipid and phospholipid content was carried out on the same tissues to establish a correlation between spectral features and biochemical composition.

2.4.1 Total protein estimation: Folin-Lowry assay, proposed by Oliver H. Lowry in 1951, one of the most commonly used methods of protein estimation was employed [36]. This method is based on two chemical reactions. The first reaction is the reduction of copper ions under alkaline conditions, which forms a complex with peptide bonds (Biuret reaction). The second is the reduction of Folin-Ciocalteu reagent by the copper-peptide bond complex, which subsequently causes a color change of the solution. It gives the dark blue to purplish and can be measured at any wavelength between 650 nm and 750 nm with little loss of intensity. It is best to measure the color at 750 nm since it is more sensitive as very few other substances absorb light at this wavelength. Tumor and normal tissues were homogenized in appropriate buffer. A standard curve was plotted by employing varying concentrations of BSA. The procedure is as follows: One hundred µl of either blank/ standard (5-40 µg BSA solution)/ sample (tissue homogenate) were taken in test tubes. To this, 1 ml of freshly prepared CTC solution (0.8 N NaOH, 10% sodium dodecyl sulphate (SDS) in D/W) was added and the tubes were vortexed for thorough mixing. After incubation at RT for 10 min, 500 µl of FC reagent (1:6 dilution) was added. The tubes were vortexed and incubated in the dark for 30 min at RT. All samples and standards were run in duplicates. The concentration of protein (expressed per mg of tissue weight) in the samples was determined from the standard curve.

2.4.2 Total lipid estimation: The total lipid content of the tissues was estimated using the protocol of Floch *et al*. [37]. In this method first the tissue was homogenized in chloroform/methanol (2/1) mixture in a final volume 20 times to the volume of the tissue sample (*e.g.*1g in 20 ml of solvent mixture). After dispersion, the whole mixture was agitated for 15-20 minutes in an orbital shaker at room temperature. The liquid phase of the homogenate was recovered after centrifugation at 1000 rpm for 15 minutes. This was followed by washing with 0.2 volumes (4 ml for 20 ml) of 0.9% sodium chloride (NaCl) solution. After vortexing the mixture was centrifuged at low speed (2000 rpm) to separate the two phases. The upper phase was removed by siphoning. The remaining solvent along with the interface was washed with methanol/water (1/1) solution without mixing the whole preparation. The lower chloroform phase containing lipids was evaporated under a nitrogen stream and lipid content was expressed per mg tissue weight.

2.4.3 Phospholipid estimation: Estimation of phospholipids was performed by the method of Rouser *et al.* [38]. This method is based on the principle of converting the organic phosphorus to inorganic phosphorus, which on reaction with ammonium molybdate, forms phosphomolybdic acid. This in turn, on reduction with ascorbic acid, forms a stable color which can be read optically at 800 nm. Dried total lipid samples and standards (1 to 5 µg P/tube) were dissolved in 0.65 ml perchloric acid and placed in heated block for about 30 minutes or until the yellow color disappears. After cooling, 3.3 ml water, 0.5 ml of molybdate solution and 0.5 ml of ascorbic acid solution were added to the tubes and tubes were agitated on a vortex after each addition. The tubes were placed in a boiling water bath for 5 minutes and the absorbances of cooled samples (including the standards) were read at 800 nm using the spectrometer (U-2001, Hitachi, Japan). Amount of phospholipids were calculated using the standard curve and expressed in per mg of tissue weight.

3. Results and Discussion

3.1 Mean spectra

The mean spectra along with standard deviation of normal and tumor tissues are shown in Figure 1A and B, respectively. Architectural arrangements of different layers are considered as the hallmark of spectral profile. The spectral features observed in the present study corroborates with the profiles noted in our earlier reports [19-30]. Origin of lipid rich features in normal tissues has been primarily attributed to the architectural arrangement of different layers. Under normal conditions, clear stratification between different layers like epithelium (superficial), lamina propria (sub epithelial connective tissue) and submucosa (deeper portion of connective tissue) can be seen. Biochemically, the lamina propria contains reticulin and collagen fibers, while the submucosa is rich in adipose tissue. This is supported by predominant lipid signatures e.g. ester bands (1744 cm^{-1}), strong δCH_2 bend (1440 cm^{-1}), two sharp features around amide III and a sharp peak around 1440 cm^{-1} seen in the mean normal spectrum. Therefore relatively weak and sharp band around 1650 cm^{-1} in normal tissues has been assigned to C=C modes of lipids. In case of tumors, there is a loss of architectural arrangement of the different layers, therefore content of different layers are mixed and lipid features are not seen. Additionally in case of malignancy, cells have large amounts of surface proteins, like receptor proteins, enzymes, antigens, and

antibodies, which may lead to a protein-dominated spectrum as indicated by broad amide III, broadened δCH_2, strong and broad features in the amide I region.

3.2 Curve-Deconvolution

In conventional or macro Raman spectroscopy, the spectra are acquired over a large probing area (20-100 μm) and represent gross information e.g. spectra in the present study were acquired over an area of 105 μm. It is also well known that a spectrum is an envelope of different bands arising from various biochemical constituents for complex biological samples. For example amide III region (1200-1400 cm^{-1}) of any biological sample can have mixture of bands arising from disordered proteins, α-helix, β-sheet of proteins, collagen, lipids and DNA. By utilizing proper data mining tools - *e.g.* spectral subtraction or multivariate analysis (principal component analysis, linear discriminant analysis, etc.), correlation of Raman spectra with biochemical components can be achieved. Curve deconvolution is one such method. The goal of curve deconvolution is to mathematically create individual peaks from a spectrum that, when added together, match the original data. Using an optimal fitting function, spectra are resolved into individual components and peak parameters such as location (frequency), height (intensity), FWHM and area under band can be obtained [22-24]. In this method second derivative calculation is done first to identify the possible number of peaks existing in a data set/spectrum. The number of distinct minima for the second derivative and their position gives a good indication about peak number and location. It is followed by identifying optimum fitting functions *i.e.* Gaussian, Lorentizian or mixed. In our analysis Gaussian function led to best fit. Spectra were interpolated to specific ranges (δCH_2 and amide I region) and curve deconvolution utilizing Gaussian function was performed (Figure 2 and 3). The spectra after curve deconvolution (FT), residual (R) depicting differences between the original and fitted spectra, and 2nd derivative spectra (2D) indicating exact peak positions were also generated.

Raman bands at 1430 cm^{-1} (CH_2 scissoring), 1443 cm^{-1} (CH_2 and CH_3 deformation of lipids and triglycerides), 1453 cm^{-1} (C-H bending of lipids, amino acids side chains) and 1480 cm^{-1} (C=N stretching of nucleic acids) in normal and tumor spectrum were fitted in the δCH_2 region (1400-1500 cm^{-1}) (Figure 2A,B and Figure 3A,B). Four bands at 1620 cm^{-1} (Trp (IgG), Phe, Tyr), 1660 cm^{-1} (amide I vibration mode of structural proteins, ν(C=C)cis lipids, fatty acids), 1680 cm^{-1} (amide I, β-sheet) and 1750 cm^{-1} (C=O esters of lipids and fatty acids) were

fitted in the amide I region (1600-1800 cm^{-1}) of normal spectrum (Figure 2C,D). Five bands at 1540 cm^{-1} (heme and aromatic hydrogens), 1590 cm^{-1} (C=N and C=C stretching in quinoid ring), 1628 cm^{-1} (amide C=O stretching for the β-form polypeptide films), 1655 cm^{-1} (amide I vibration mode of structural proteins, *ν*(C=C)cis lipids, fatty acids) and 1690 cm^{-1} (amide I disordered structures, β-sheet) were fitted in the tumor spectrum in the 1500-1800 cm^{-1} range (Figure 3C,D). The average intensity of the lipid band (1440 cm^{-1}) in normal and tumor tissues was 1.42 $\pm$ 0.25 and 0.43$\pm$0.18, respectively (Figure 4A and Table 1). This difference was found to be statistically significant by unpaired student's t-test ($p < 0.0001$). The average intensity of the protein band (1450 cm^{-1}) was high in tumors (1.46$\pm$0.29) as compared to normal (0.51$\pm$0.12) (Figure 4B and Table 1). Again, this difference was found to be highly significant ($p < 0.0001$). The average intensity associated with the other protein band (1660 cm^{-1}) in the amide I region was also computed. Statistically significant difference (p value = 0.004) between normal (0.89$\pm$0.28) and tumor (1.12$\pm$0.19) tissues (Figure 4C and Table 1) was observed. In order to determine if the band intensity parameters can be explored for classification, scatter intensity plots of lipid (1440 cm^{-1}) against protein bands (1450 cm^{-1} and 1660 cm^{-1}) were generated (Figure 4D and 4E). Two separate clusters indicating higher intensity of lipid band (1440 cm^{-1}) were obtained in normal tissues as compared to tumor tissues. Similarly, the intensity of the protein bands (1450 cm^{-1} and 1660 cm^{-1}) was high in case of tumors (Figure 4D and 4E).

3.3 Biochemical estimations

The presence of tumor in the body produces a number of deleterious effects such as anorexia, nausea, impaired digestion and cachexia in the host which leads to variety of biochemical differences among normal and malignant cells. Cancer cells show a variety of alterations on the cell surface and also display disturbed arrangement of the cell membrane, as compared to their normal counterparts. The alteration in membrane lipids is considered as an important aspect of malignant transformation. In the next step, to verify if the spectral markers can serve as biochemical markers, estimation of total lipid, total protein and phospholipid was performed using the same tissues. The protein to lipid and phospholipid ratio was calculated. As shown in Figure 5A and Table 1, protein to lipid ratio was high in case of tumors (2.15$\pm$0.41) with respect to normal tissues (0.72$\pm$0.22). When unpaired student's t-test was performed, a statistically significant difference ($p < 0.0001$) was observed. As can be seen from Figure 5B and Table 1,

protein to phospholipid ratio yielded similar and significant results *i.e.* high in tumors (24.13±2.12) and low in normal (16.12±2.28).

3.4 Correlation of curve-deconvolution and biochemical estimations

Mean spectral profile of normal tissues indicates predominance of lipids while tumor spectra are rich in proteins. These features corroborate the spectral profile noted in our earlier reports [21-30]. Curve-deconvolution procedures can help in resolving overlapping bands which can lead to better interpretation and correlation of biochemical constituents. Similar to features observed in the mean/average spectra, intensity associated with protein bands was high in case of tumors (1.46±0.29 and 1.12±0.19) while that of lipid band was high in normal (1.42 ± 0.25), Table 1. However, in view of variable Raman scattering cross-section it is also important to analyze spectral features with respect to tissue biochemical composition to correlate spectral markers as biochemical markers. As can be seen from Table 1, Corroborating mean spectral profile and findings of curve-deconvolution analysis, biochemical estimation yielded similar results *i.e.* protein to lipid ratio was high in case of tumors (2.15±0.41) and *vice versa* for normal (0.72±0.22). Origin of these features in normal tissues is primarily attributed to the architectural arrangement of different layers. In case of pathological conditions cells contain large amounts of surface proteins, receptor proteins, enzymes, antigens and anti-bodies which might be responsible for the protein dominated spectrum. In addition to the deleterious effects described earlier lipids are also required for maintaining cell shape, signaling and various cell processes. Polyunsaturated fatty acids are the major class of biomolecules susceptible to oxidative damage by reactive oxygen species generated by tobacco exposure. This could be one of the reasons for the decreased amounts of lipids in cancerous conditions, as suggested by Raman spectra and confirmed by biochemical estimation. A decrease in the phospholipid concentration can be attributed to dysfunction of the cell membrane in malignancy leading to an increase in phospholipid degradation.

4. Conclusions

Raman spectra are sensitive towards histological or biochemical variations associated with disease onset. Histopathological and Raman spectra correlation are well documented. In the present study biochemical variations *viz a viz* Raman spectra have been investigated. Gross spectral features, intensity of curve-resolved protein/lipid bands and biochemical estimation

suggest that the lipid to protein ratio is high in normal tissue and *vice versa* in tumors. Overall findings of this study indicate that, spectral features are the true representative of underlying biochemical make-up of a tissue and supports utility of protein to lipid ratio as a prospective spectral and biochemical marker for oral cancer diagnosis.

Acknowledgements

This work, carried out under Project No. BT/PRI11282/MED/32/83/2008 Department of Biotechnology, Government of India. The authors would like to acknowledge the help received from Mrs. Arti R. Hole in histopathological analysis of tissues. The contribution of Dr. Gaurav Kumar and Dr. G.B. Maru in biochemical analysis is also acknowledged. Editorial makeover of the manuscript by Dr. A. Bagwe, SCOPE Cell, ACTREC and Ms. Aditi Sahu is gratefully acknowledged.

References

1. American Cancer Society. Cancer Facts & Figures 2012. Atlanta: American Cancer Society; (2012)
2. J Ferlay, HR Shin, F. Bray, D. Forman, C. Mathers, D. Parkin, *Int J Cancer.* 127, 2893–2917 (2008).
3. D.M. Saman, *Head & Neck Oncology*, 4,1-7 (2012).
4. R Dikshit, PC Gupta , C Ramasundarahettige , V Gajalakshmi, L Aleksandrowicz , R Badwe, R Kumar, S Roy , W Suraweera , F Bray , Mallath M, PK Singh, DN Sinha , Shet AS, Gelband H, Jha P, *Lancet*. 379,1807-1816 (2012).
5. P. Boffetta, S. Hecht, N. Gray, P. Gupta and K. Straif, *The Lancet Oncology,* 2008, 9, 667–75.
6. B Mathew, R Sankaranarayanan, KB Sunil kumar, P Pisani, M Krishnan Nair, *Br J Cancer,*76, 390-394 (1997).
7. L.M. Abbey, G.E. Kaugars, J.C. Gunsolley, J.C. Burns, D.G. Page, J.A. Svirsky, E. Eisenberg, D.J. Krutchkoff, M. Cushing, *Oral Surg Oral Med Oral Pathol Oral Radiol Endod,* 80, 188-191(1995).
8. D.C. De Veld, M.J. Witjes, H.J. Sterenborg, J.L. Roodenburg, *Oral Oncol,* 4, 117-131(2005).
9. J.G. Wu, Y.Z Xu, C.W. Sun, R.D. Soloway, D.F. Xu, Q.G. Wu, K.H. Sun, S.F. Weng, G.X. Xu, *Biopolymers*, 48,167-175 (2005).
10. P. Crow, B. Barrass, C. Kendall, M. Hart-Prieto, M. Wright, R. Persad, N. Stone *Br J Cancer* 92, 2166-2170 (2005).
11. G. Shetty, C. Kendall, N. Shepherd, N. Stone, H. Barr, *Br J Cancer* 94, 1460-1464 (2006).
12. S. Duraipandian, M. Sylvest Bergholt, W. Zheng, K. Yu Ho, M. Teh, K. Guan Yeoh, J. Bok Yan So, A. Shabbir , Z. Huang, *J Biomed Opt* 17, 081418 (2012).
13. Z. Huang, Z., S. K. Teh, W. Zheng, K. Lin, K. Y. Ho, M. The, K. G. Yeoh, *Biosens Bioelectron* 26,383-389 (2010).
14. E.M. Kanter, E. Vargis, S. Majumder, M. D. Keller, E. Woeste, G. G. Rao, A. Mahadevan-Jansen , *J Biophotonics* 2, 81-90 (2009).

15. S. Koljenovic, T. C. Bakker Schut, R. Wolthuis, B. de Jong, L. Santos, P. J. Caspers, J. M. Kros, G. J. Puppels, *J Biomed Opt* 10,031116 (2005).

16. M.D. Morris, G. S. Mandair2011), *Clin Orthop Relat Res,* 469, 2160-2169 (2011).

17. J. Popp, C. Krafft T. Mayerhöfer, *Optik & Photonik* 6,24-28 (2011).

18. T. Meyer, N. Bergner, C. Bielecki, C. Krafft, D. Akimov, B. F. M. Romeike, R. Reichart, R. Kalff, B. Dietzek, J. Popp, *J Biomed Opt* 16,021113-021110 (2011).

19. K. Venkatakrishna, J. Kurien, K.M. Pai, C. Murali Krishna, G. Ullas, V.B. Kartha, *Curr. Sci,* 80, 101-05(2001).

20. C.M. Krishna, G.D. Sockalingum, J. Kurien, L. Rao, L. Venteo, M. Pluot, M. Manfait, V.B. Kartha, *Appl Spectrosc*,58, 1128-1135 (2004).

21. R. Malini, K. Venkatakrishna, J. Kurien, K. M. Pai, L. Rao, V. B. Kartha, and C. M. Krishna, *Biopolymers*, 8, 179-193 (2006).

22. K. Guze, M. Short, S. Sonis, N. Karimbux, J. Chan, H.Zeng, *J Biomed Opt,* 140, (2009).

23. H. Zhiwei , K.T. Seng, Z. Wei, M. Jianhua, L. S Kan, Xiaozhuo, Y.H. Khek, T. Ming, G.Y. Khay, *Opt Lett,* 34, 758-760 (2009).

24. A.T. Harris , A. Rennie , H. Waqar-Uddin , S.R. Wheatley , S.K. Ghosh , D.P. Martin-Hirsch, S.E. Fisher , A.S. High , J. Kirkham , T. Upile, *Head & Neck Oncology,* 2, 1-6(2010).

25. SP Singh, A. Deshmukh, P Chaturvedi, CM Krishna, *J Cancer Res Ther.* 8, 126-132 (2012).

26. SP Singh, A. Deshmukh, P. Chaturvedi, CM Krishna, *Proc. of SPIE,* 8219, K1-K6(2012).

27. SP Singh, A. Deshmukh, P Chaturvedi, CM Krishna, *J Biomed Opt,* 17,21-29(2012).

28. SP Singh, Aditi Sahu, A. Deshmukh, P. Chaturvedi, CM Krishna, *Analyst,*138, 4175-4182 (2013).

29. A Sahu, A. Deshmukh. AD Ghanate, SP Singh, P. Chaturvedi, CM Krishna, *Technol Cancer Res Treat*, 1, 529-541(2012).

30. A. Deshmukh, SP Singh, P Chaturvedi and C M Krishna, *J. Biomed. Opt.,*16, 127004-10 (2011).

31. A. S. Haka, KE. Safer-Peltier, M Fitzmaurice, J Crowe, RR. Dasari, and MS Feld, *PNAS* 102, 12371-12376 (2005).

32. MV Chowdary , Kalyan Kumar K, S Mathew , L Rao , CM Krishna , Kurien J, *Biopolymers.*

9, 539-546(2009).

33. MV Chowdary , KK Mahato , Kumar KK, S Mathew , L Rao , CM Krishna, J. Kurien, *Photomed Laser Surg*, 27, 241-252 (2009).

34. PLS plus/IQ User's Guide; Galactic Industries Corporation, 1999

35. D. W. Marquardt, *J. Soc. Ind. Appl. Math.*, 11, 431-441 (1963).

36. OH Lowry , NJ Rosebrough , AL Farr , RJ Randall , *J Biol Chem*, 193, 265-275(1951).

37. Folch J, M Lees, GH Sloane, *J Biol Chem,* 226, 497–509 1957).

38. Rouser G, Fkeischer S, Yamamoto A, *Lipids.* 5, 494-496(1970).

Table 1: Raman intensity and Biochemical estimation of protein, lipids and phospholipids of normal and tumor tissues

	Normal (n=20)		Tumor (n=20)	
	Raman intensity	**Biochemical estimation**	**Raman intensity**	**Biochemical estimation**
Protein	0.51±0.12 (1450 cm^{-1}) 0.89±0.28 (1660 cm^{-1})	0.28±0.08 (Protein / Lipid) (0.72±0.22)	1.46±0.29 (1450 cm^{-1}) 1.12±0.19 (1660 cm^{-1})	0.62±0.12 (Protein / Lipid) (2.15±0.41)
Lipid	1.42 ± 0.25 (1440 cm^{-1})	0.37±0.45 (Protein / Lipid) (0.72±0.22)	0.43±0.18 (1440 cm^{-1})	0.28±0.59 (Protein / Lipid) (2.15±0.41)
Phospholipid	**NA**	0.016±0.11 (Protein / Phospholipid) (16.12±2.28)	**NA**	0.025±0.28 (Protein/Phospholipid) (24.13±2.12)

Figure legends

Figure 1: Mean / average spectra along with standard deviation of normal (A) and tumor (B) oral biopsies. (Solid line: mean spectra; dotted line: positive standard deviation; broken line: negative standard deviation)

Figure 2: Curve deconvolution of normal spectra in CH_2 region (A-B) and amide I region (C-D). (2D – 2nd Derivative; FT- Fitted trace; R- Residual)

Figure 3: Curve deconvolution of tumor spectra in CH_2 region (A-B) and amide I region (C-D). (2D – 2nd Derivative; FT- Fitted trace; R- Residual)

Figure 4: Average intensity of Raman bands in normal (empty bar) and tumor (shaded bar). (A) lipid band (1440 cm^{-1}); (B) Protein band (1450 cm^{-1}); (C) Protein band (1660 cm^{-1}); (D) Scatter intensity plot of lipid bands (1440 cm^{-1}) and protein (1450 cm^{-1}) (E) Scatter intensity plot between lipid (1440 cm^{-1}) and protein band (1660 cm^{-1}) [△-Normal , ●- Tumor].

Figure 5: Biochemical estimation of protein and lipids in normal (empty bar) and tumor (shaded bar). (A) Ratio of total protein to total lipid; (B) Ratio of total protein to phospholipid.

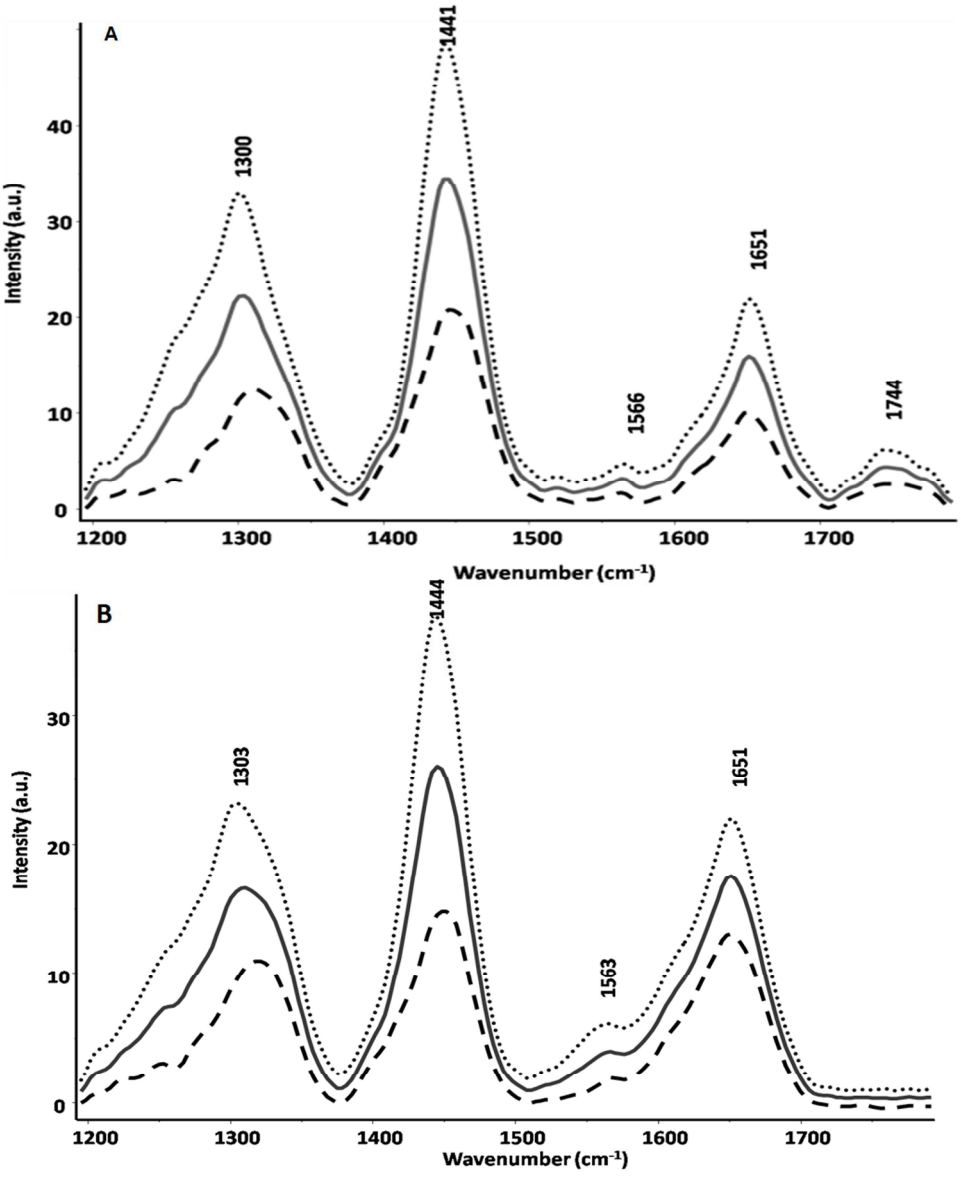

Mean / average spectra along with standard deviation of normal (A) and tumor (B) oral biopsies. (Solid line: mean spectra; dotted line: positive standard deviation; broken line: negative standard deviation)
285x338mm (300 x 300 DPI)

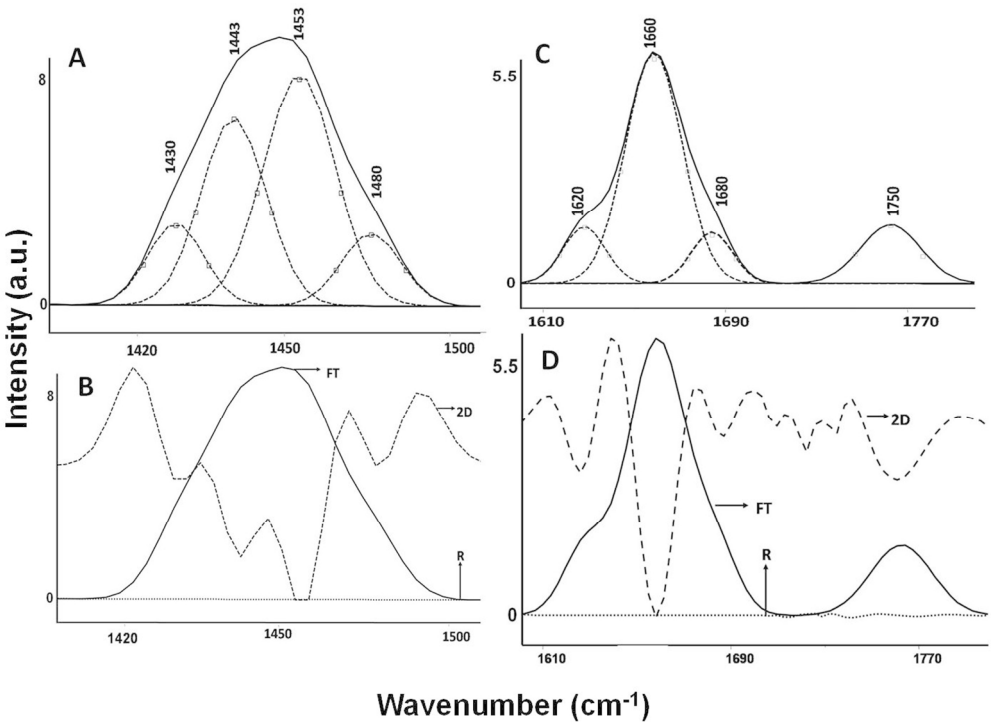

Curve deconvolution of normal spectra in CH2 region (A-B) and amide I region (C-D). (2D – 2nd Derivative; FT- Fitted trace; R- Residual)
172x124mm (300 x 300 DPI)

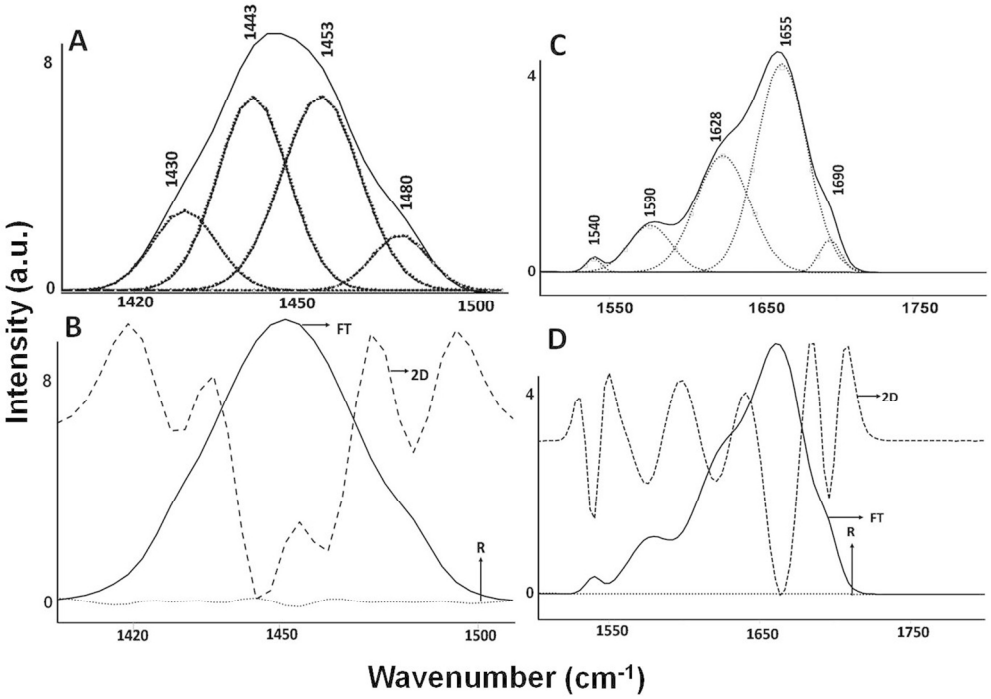

Curve deconvolution of tumor spectra in CH2 region (A-B) and amide I region (C-D). (2D – 2nd Derivative; FT- Fitted trace; R- Residual)
163x114mm (300 x 300 DPI)

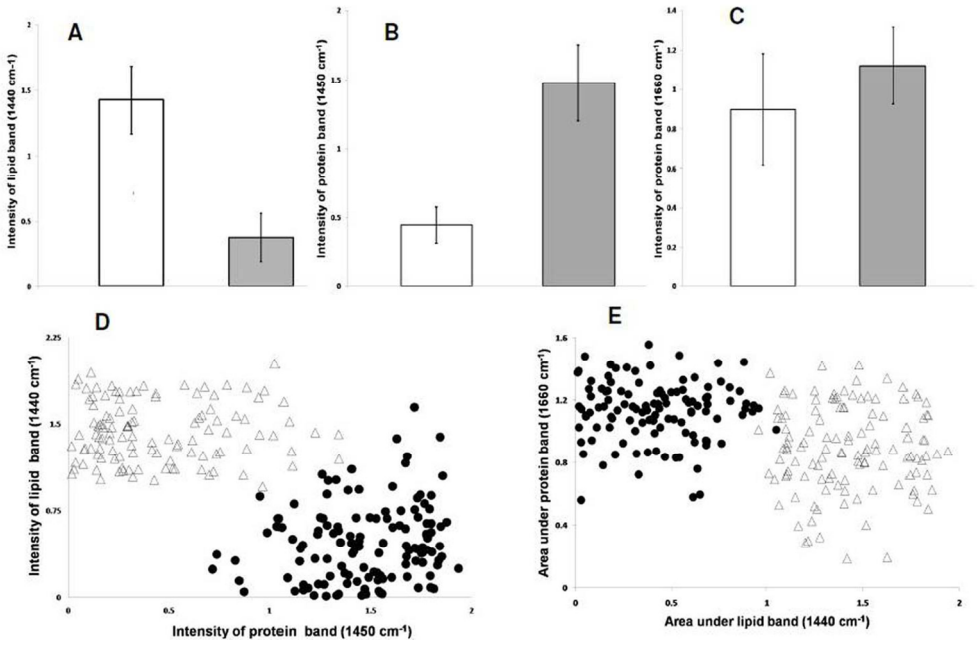

Average intensity of Raman bands in normal (empty bar) and tumor (shaded bar). (A) lipid band (1440 cm-1); (B) Protein band (1450 cm-1); (C) Protein band (1660 cm-1); (D) Scatter intensity plot of lipid bands (1440 cm-1) and protein (1450 cm-1) (E) Scatter intensity plot between lipid (1440 cm-1) and protein band (1660 cm-1) [-Normal , - Tumor].

162x105mm (300 x 300 DPI)

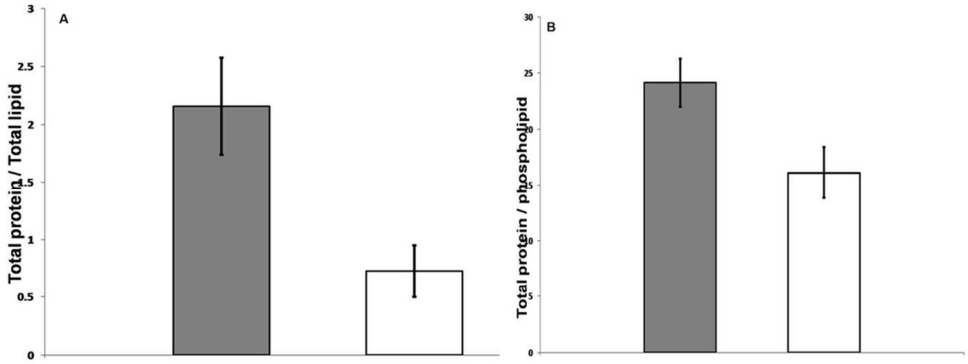

Biochemical estimation of protein and lipids in normal (empty bar) and tumor (shaded bar). (A) Ratio of total protein to total lipid; (B) Ratio of total protein to phospholipid.
97x38mm (300 x 300 DPI)